fracture probability F is a function of the dynamic shape and scaling parameters m and σ_0 ($F = 1 - \exp\{-(\sigma/\sigma_0)^m\}$; σ = stress). Again, the exploitation was performed according to IEC 793-1-3 [7]. Our results are plotted in Fig. 1 and summarised in Table 1.

Table 1: Fibre rupture test results

Sample and strain rate	m-value	Median breaking strength
		GPa
Reference fibre 1mm/min	24.2	4.66
Reference fibre 10mm/min	25.1	5.25
Reference fibre 100mm/min	20.4	5.84
Gratings 1mm/min	25.8	4.71
Gratings 10mm/min	24.3	5.18
Gratings 100mm/min	28.6	5.75

For each strain rate there is nearly no difference between the Weibull distribution for the fibres with gratings and that for the fibres without gratings. It is very interesting to note that although the influence of the UV to the fibre strength is of negligible quantity, all grating samples at each strain rate broke in the grating region. This behaviour is different from the observations in [6] but may be correlated with the higher index changes achieved in our experiment. Obviously, the fibre we used exhibits a higher photosensitivity, possibly due to higher doping, and therefore high pristine internal stresses may favour fibre rupture at positions where stress is enhanced by strong interaction with UV light. For our measurements, we evaluated the dynamic (tension) stress corrosion susceptibility parameter $n_d = 19$ (95% confidence interval $16.3 < n_d < 23.9$) for the reference fibres and $n_d = 23.9$ (95% confidence interval $19.3 < n_d < 31.0$) for the grating fibres. Within the confidence interval, which is rather wide due to the limited number of samples, these values are of the same magnitude and have the same quantity as for standard telecommunication fibres (typically > 20).

Conclusions: Fibre strength measurements according to IEC 793-1-3 were performed on draw-tower FBGs, including the evaluation of the stress corrosion susceptibility parameter. The FBGs suffer nearly no loss of strength, even though we wrote gratings with an index modulation more than three times higher than those in [6]. This emphasises the fact that it is favourable to use draw-tower FBGs as sensor elements to overcome the problem related to fibre stripping and high fluence UV-irradiation. Work is continuing to increase the grating reflectivities, to test the permanent load and alternating stress, and to use other types of coatings which are more suitable for sensor applications than acrylat coatings.

Acknowledgments: We thank FibreCore Jena GmbH, Germany for preparing the preform for the highly photosensitive fibre. The work at the IPHT and at FibreCore Jena was supported by the German government (BMBF FKZ 01 BP 450/2) and by the Daimler Benz AG, Germany.

29 August 1997
Electronics Letters Online No: 19980136

V. Hagemann, M. Rothhardt and H.-R. Müller (*Institute for Physical High Technology e.V.-IPHT, Modern Optics Division, Helmholtzweg 4, 07743 Jena, Germany*)

M.N. Trutzel, L. Staudigel and O. Krumpholz (*Daimler Benz Research and Technology, Highfrequency Laboratory (FT2), Wilhelm-Runge-Strasse 11, 89081 Ulm, Germany*)

References

1 DONG, L., ARCHAMBAULT, J.-L., REEKIE, L., RUSSELL, P.St.J., and PAYNE, D.N.: 'Single pulse Bragg gratings written during fibre drawing', *Electron. Lett.*, 1993, **29**, (17), pp. 1577–1578

2 ASKINS, C.G., PUTNAM, M.A., WILLIAMS, G.M., and FRIEBELE, E.J.: 'Stepped-wavelength optical fibre Bragg grating arrays fabricated in line on a draw tower', *Opt. Lett.*, 1994, **19**, (2), pp. 147–149

3 WEI, T., YUEE, H.H., HASZ, C.H., and KEY, P.L.: 'Degradation of fibre strength during coating stripping'. Int. Wire & Cable Symp. Proc., 1989, pp. 199–204

4 VARELAS, D., LIMBERGER, H.G., SALATHÉ, R.P., and KOTROTSIOS, C.: 'UV-induced mechanical degradation of optical fibres', *Electron. Lett.*, 1997, **33**, (9), pp. 804–806

5 FECED, R., ROE-EDWARDS, M.P., KANELLOPOULOS, S.E., TAYLOR, N.H., and HANDEREK, V.A.: 'Mechanical strength degradation of UV exposed optical fibres', *Electron. Lett.*, 1997, **33**, (2), pp. 157–159

6 ASKINS, C.G., PUTNAM, M.A., PATRICK, H.J., and FRIEBELE, E.J.: 'Fibre strength unaffected by on-line writing of single-pulse Bragg gratings', *Electron. Lett.*, 1997, **33**, (15), pp. 1333–1334

7 International Electrotechnical Commission (IEC), International Standard (CEI-IEC 793-1-3), Optical fibres, 1995

Retracing behaviours of a BBO optical parametric oscillator pumped with 532nm laser

Chih-Wei Hsu, S.D. Huang, D.W. Huang and C.C. Yang

The authors report experimental results of the retracing behaviours in a BBO optical parametric oscillator pumped by the second harmonic of a Q-switched Nd:YAG laser. Two sets of signal-idler could be observed in their noncolinear type-I phase-matching configuration in a certain tuning range. Particularly, near the turning point of phase-matching angle, they have implemented simultaneous phase matching for a broad wavelength range. In this situation, the spectral width of the signal output can be as large as 160nm (740–900nm), and that of the idler is 590nm (1.3–1.89μm). With a tuning setup, such as a grating, broadly tunable coherent sources can be obtained in the above wavelength ranges without a complicated tuning mechanism.

The retracing behaviour of the phase-matching angle, which is the key to realising multi-wavelength optical parametric oscillators (OPO), was first reported in LBO by Lin *et al.* [1, 2] and was also studied by Liu *et al.* [3] in other crystals. In their studies, only OPOs with colinear phase matching were considered and the retracing phenomena could be observed only within certain ranges of pumping wavelength in which high-power lasers are not available for pumping. Previously, multi-wavelength OPO [4] and optical parametric amplifiers [5] were implemented only in LBO crystals because the range of eligible pumping wavelength includes 532 and 523nm (the second-harmonic of Nd:YAG and Nd:YLF lasers, respectively). In this Letter, we experimentally show, for the first time, that BBO can also be used for observing retracing behaviours with 532nm pumping (not in the eligible pumping range described in [3]) in noncolinear phase-matching configurations. Actually, our numerical studies also show that BBO OPOs can result in retracing behaviours when pumped with any harmonic of a Nd:YAG laser (not reported here).

Our OPO cavity consisted of two plane mirrors which were coated near 810 nm with reflectivities of 99.5 and 98% (output coupler), respectively. The cavity length was 2.5cm. The pumping source was the second harmonic of a single-longitudinal-mode, *Q*-switched Nd: YAG laser (coherent infinity 40–100). The laser was operated at the repetition rate 10Hz. The threshold pump pulse energy of 532nm for oscillation was ~ 12mJ/pulse. The pump pulse was 5ns in duration and had a top-hat spatial profile. We used a two-time telescope for reducing the beam diameter to 2.75mm. The BBO crystal with dimensions 10mm × 8mm × 7mm was cut for type-I phase matching ($\theta = 20°$, $\phi = 0°$). Both type-I and type-II phase matching interactions are feasible. However, type-I phase matching has a higher parametric gain. Its facets were AR-coated at 810nm.

Fig. 1 demonstrates the phase matching condition within the crystal for a noncolinear configuration. Since BBO is a negative uniaxial crystal, the pump beam must be an extraordinary wave; the signal and idler are ordinary waves for type-I phase matching ($e \rightarrow o + o$). The Poynting vector of pump $\mathbf{P}_p$ differs from $\mathbf{K}_p$ (wave vector of the pump) due to walk-off. If $\mathbf{K}_s$ (wave vector of the signal) is parallel to $\mathbf{P}_p$ (then $\mathbf{P}_s$ overlaps with $\mathbf{P}_p$ because the signal is an ordinary wave), we can obtain the maximum parametric gain for the OPO. The advantages of a noncolinear configura-

tion include low threshold and high conversion efficiency [6]. However, the drawbacks include broader spectral bandwidth and a poor spatial mode for the idler beam. The degree of noncolinearity is determined by the magnitude of the angle α (the air angle between pump and signal).

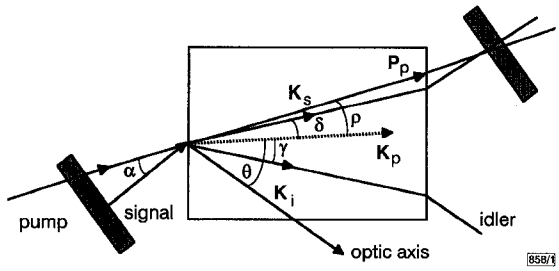

Fig. 1 *Diagram showing phase-matching in noncolinear OPO cavity*

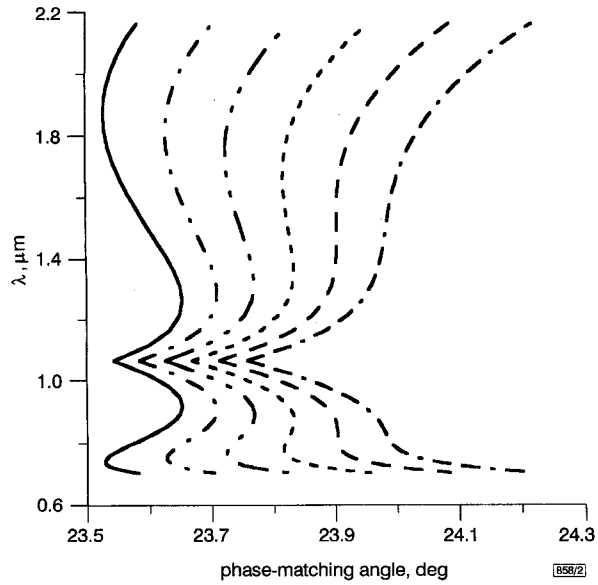

Fig. 2 *Theoretical phase-matching angle pumped with 532 nm*

BBO crystal is cut at θ = 20°
α (deg):
——— 3.7
— · — · 3.8
— — — — 3.9
– – – – – 4.0
— — — 4.1
— — · —4.2

Fig. 2 shows the theoretical predictions of phase-matching angle θ with α = 3.7° – 4.2° which is pumped with 532nm. The retracing behaviours are clear for α in this range (actually, retracing can be observed with α = 2°–4°). However, since our cavity coating limits usable wavelengths, it is difficult to experimentally follow the whole retracing behaviours. Nevertheless, around the coating wavelength, we could still observe the simultaneous oscillation of two sets of signal-idlers. Fig. 3 shows the experimental spectrum with two bands of signal wavelength. The results were obtained with α = 3.9° amd 20mJ/pulse pump energy. According to the theory, the peaks of the two bands should be at 728 and 894nm, respectively. However, the coating range limits the observation of the whole spectrum.

From Fig. 2, we can observe that when α is close to 4.1°, the phase-matched curve becomes almost vertical in the signal wavelength range 0.8–0.9μm. This means that we can obtain a broad signal bandwidth from the phase-matched OPO if θ and α are appropriately chosen. Fig. 4 shows the experimental results when α is close to 4.1° and the pump energy is ~ 30mJ/pulse. Here, we show four spectra, indicating that when θ is slightly decreasing the centre of the signal spectral band shifts from the short to long wavelength end (dashed, solid, dash-dot-dotted and dash-dotted curves, accordingly). These results are consistent with our theoretical predictions. Among the four curves in Fig. 4, the dash-dot-dotted curve has effectively the broadest bandwidth ranging from 740 to 900nm. The corresponding idler range is from 1.3 to 1.89μm. The spectral widths of the signal and idler are as large as 160 and 590nm, respectively. These spectral widths are actually limited by the cavity mirror coating. Even broader spectral widths can be expected if the coating range can be enlarged. If we use a tuning setup, such as a grating, we can obtain broadly tunable coherent sources in the above wavelength ranges without complicated tuning arrangements. Recently, a similar broad spectral width BBO OPO was also implemented with 355nm pumping [7].

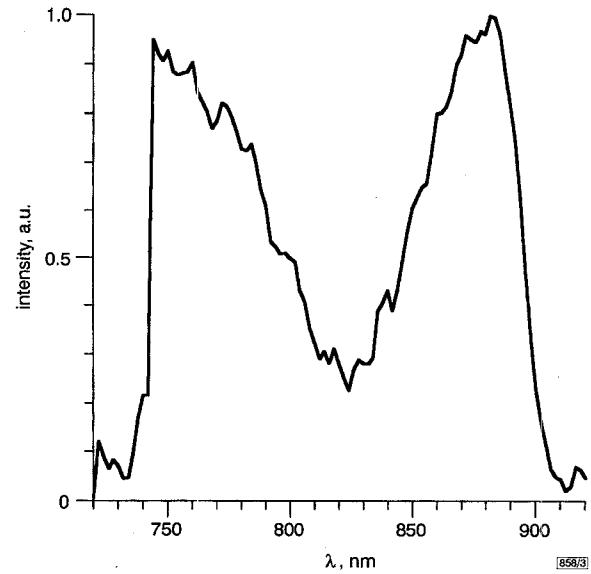

Fig. 3 *Signal spectrum of OPO*

The two separate bands indicate retracing behaviour

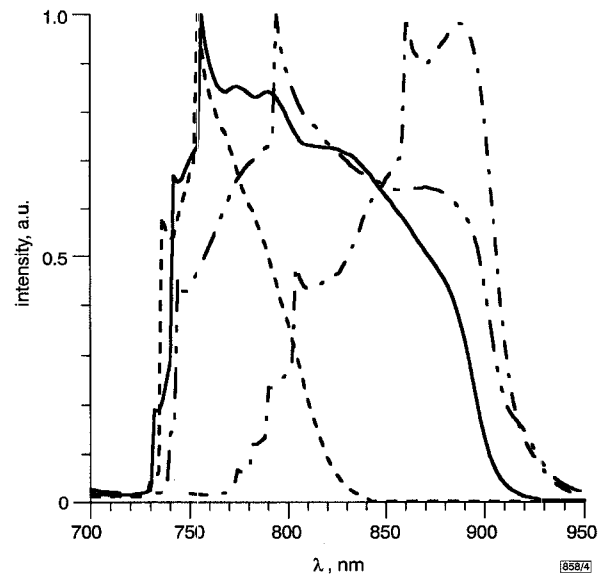

Fig. 4 *Signal spectra OPO for four slightly different phase-matching angles*

In summary, we have experimentally shown that the retracing behaviours of a BBO OPO could be observed in a noncolinear configuration when pumped with the second harmonic of a Nd:YAG laser. The experimental results were consistent with our theorical predictions. Limited by our cavity mirror coating, we could observe two separate signal bands. Meanwhile, we also reported broad signal and idler spectral widths when the phase-matching angles were appropriately adjusted. We have demonstrated an OPO system from which the spectral widths of the signal and idler can be as large as 160 and 590nm, respectively. A drawback of such a system is that the idler spreads in space for several degrees. Therefore, it is difficult to collect the whole idler signal with a simple setup.

Acknowledgment: This research was sponsored by grants NSC 86-2215-E-002-010 and NSC 86-2215-E-002-011 from National Science Council, The Republic of China.

5 August 1997
Electronics Letters Online No: 19980183

Chih-Wei Hsu, S.D. Huang, D.W. Huang and C.C. Yang (*Institute of Electro-Optical Engineering and Department of Electrical Engineering, National Taiwan University, 1, Roosevelt Road, Sec. 4, Taipei, Taiwan, Republic of China*)

E-mail: ccy@cc.ee.ntu.edu.tw

References

1 LIN, S., WU, B., XIE, F., and CHEN, C.: 'Phase-matching retracing behaviour: New features in LiB_3O_5', *Appl. Phys. Lett.*, 1991, **59**, pp. 1541–1543
2 LIN, S., WU, B., XIE, F., and CHEN, C.: 'Phase-matching retracing behaviour for second harmonic generation in LiB_3O_5 crystal', *J. Appl. Phys.*, 1993, **73**, pp. 1029–1034
3 LIU, X., DENG, D., LI, M., GUO, D., and XU, Z.: 'Retracing behaviour of the phase-matching angle of nonlinear crystals in optical parametric oscillators', *J. Appl. Phys.*, 1993, **74**, pp. 2989–2991
4 HALL, G.J., EBRAHIMZADEH, M., ROBERTSON, A., MALCOLM, G.P.A., and FERGUSON, A.I.: 'Synchronously pumped optical parametric oscillators using all-solid-state pump lasers', *J. Opt. Soc. Am. B*, 1993, **10**, pp. 2168–2179
5 XU, Z., LIU, X., DENG, D., WU, Q., WU, L., WU, B., LIN, S., LIN, B., and CHEN, C.: 'Multiwavelength optical parametric amplification with angle-tuned lithium triborate', *J. Opt. Soc. Am. B*, 1995, **12**, pp. 2222–2228
6 GLOSTER, L.A.W., JIANG, Z.X., and KING, T.A.: 'Characterisation of an Nd: YAG-pumped β-BaB_2O optical parametric oscillator in collinear and noncollinear phase-matched configurations', *IEEE J. Quantum Electron.*, 1994, **30**, pp. 2961–2969
7 WANG, J., DUNN, M.H., and RAE, C.F.: 'Polychromatic optical parametric generation by simultaneous phase matching over a large spectral bandwidth', *Opt. Lett.*, 1997, **22**, pp. 763–765

40Gbit/s high sensitivity optical receiver with uni-travelling-carrier photodiode acting as decision IC driver

Y. Miyamoto, M. Yoneyama, K. Hagimoto, T. Ishibashi and N. Shimizu

The authors demonstrate a 40Gbit/s simple optical receiver that uses a uni-travelling-carrier photodiode as a decision IC driver. The photodiode drives the decision circuit directly with 1 V_{p-p} without any electrical amplifier. Receiver sensitivity of –27.8dBm was obtained at 40Gbit/s.

Introduction: An ultra-high speed EDFA-based receiver can be simply achieved by introducing a high power photodiode (PD) that drives the digital decision circuit directly [1]. All electrical gain of baseband amplifiers is converted into an optical gain of an EDFA in the receiver. This configuration makes full use of the low-noise, broadband, and high-output-power characteristic of EDFAs, and naturally requires that the PD has a high output current exceeding 20mA (50Ω), as well as a broad bandwidth. The electrically converted amplitude from a conventional *pin*-PD is optimised only for the sub-milliamperes region, and increasing the PD input power degrades the bandwidth of the *pin*-PD.

In this Letter, we first report the realisation of a 40Gbit/s photodiode driving decision circuit (PDD) optical receiver [1] that uses a uni-travelling-carrier photodiode (UTC-PD) [2]. The UTC-PD is designed for its high output power and high speed detector (>100GHz) and enables close to 100mA_{p-p} or over 2V_{p-p} amplitude output. Stable 40Gbit/s error-free-operation of a decision circuit, driven directly by a UTC-PD, was confirmed, and high sensitivity (–27.8dBm) was obtained at 40Gbit/s.

High speed and high output power characteristics of UTC-PD: Bandwidth degradation at a high output power is intrinsic to the conventional *pin*-PD structure. Low-mobility carriers, holes, cause carrier pile-up, which induces the space charge effect. This effect deforms the potential profile and prevents the carriers from moving out of the depletion layer. The UTC-PD consists of an absorption (InGaAs) and a carrier-collecting layer (InP) [2]. This PD design enables us to exploit only photo-excited electrons as active carriers in the *pin*-structure. In addition, the velocity overshoot in the InP collecting layer enhances the saturation output level.

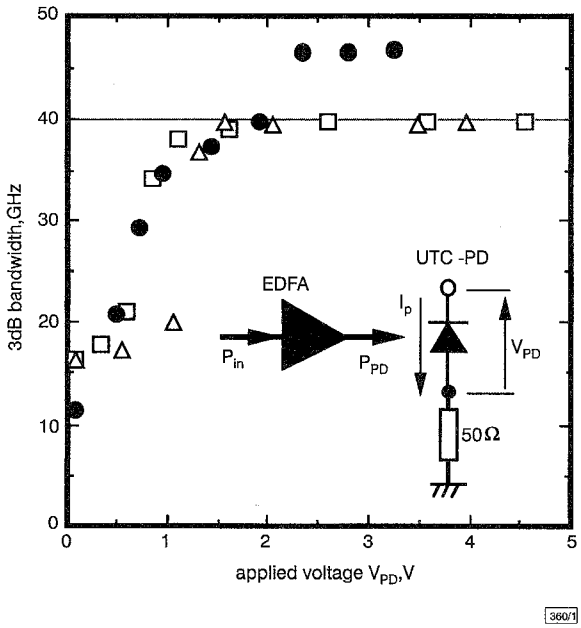

Fig. 1 *Frequency response of UTC-PD*
□ I_p = 10mA
△ I_p = 20mA
● I_p = 35mA

Fig. 1 shows the frequency response of an UTC-PD for three output current levels, where I_p is an average output current, P_{in} is an EDFA average input power, P_{PD} is the UTC-PD average input power, and V_{PD} is the applied terminal voltage of the UTC-PD. The UTC-PD module with 8.2μm ϕ receiving area showed 0.15A/W conversion efficiency at 1.55μm, including the coupling loss. The load impedance of the photodiode was 50Ω. A 3dB down bandwidth of > 40GHz was obtained for output currents up to 35mA at V_{PD} = 2V. This bandwidth is limited by a packaging and an RF microwave connector (K-connector). This result shows that UTC-PD offers broadband characteristics with high output current.

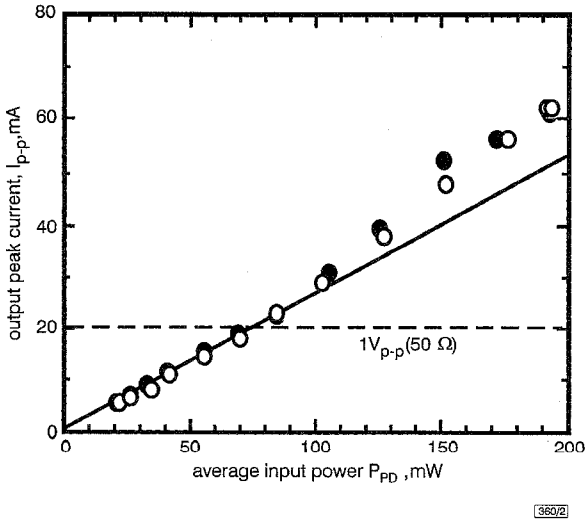

Fig. 2 *Output characteristics of UTC-PD*
● 40Gbit/s NRZ
○ 10Gbit/s NRZ

To investigate the output characteristics of the UTC-PD, peak current (I_{p-p}) measurements were conducted with the test input of non-return-to-zero (NRZ) pseudo-random signals at 10 or 40Gbit/s. The UTC-PD can drive a 50Ω load with logical amplitudes exceeding 1V_{p-p}, as shown by the dotted line in Fig. 2. Characteristic to the UTC-PD, the efficiency at 40Gbit/s was almost